Experimental Verification of Plasma Focusing by Azimuthal Current in a Magnetic Nozzle

Lorenzo Ferrario [*] , Justin M. Little [†] and Edgar Y. Choueiri [‡]

Electric Propulsion and Plasma Dynamics Laboratory

Princeton University, Princeton, NJ, 08544

The theoretically predicted ability of an applied azimuthal current to focus the plasma in a magnetic nozzle (MN) was investigated experimentally. The azimuthal current was induced through the Hall effect by applying a radial electric field with a pair of concentric electrodes upstream of the throat of an electron-driven magnetic nozzle fed by an RF plasma source. Spatially resolved probe measurements of plasma density and plasma potential inside the plasma source and in the external plume show that the induced azimuthal current leads to significant focusing of the plasma on the center axis, and is a far more efficient way to enhance the centerline density than increasing the RF power in the source. This opens the door to the potential use of a focusing stage to increase the thrust efficiency of magnetic nozzles by decreasing beam divergence.

Nomenclature

$\mathbf{B}$	Magnetic field
$\mathbf{E}$	Electric field
$\mathbf{J}$	Current density
$\dot{m}$	Mass flow rate
n	Plasma density
P	RF Power
σ	Plasma conductivity
T_i	Ion temperature
T_e	Electron tempertaure
V	Electrostatic potential

I. Introduction

A Magnetic Nozzle (MN) is a device that converts part of the thermal energy of a plasma into directed kinetic energy, with potential applications in fundamental plasma physics experiments[5], plasma processes[12] and plasma propulsion for spacecraft[1, 3, 17, 19, 21, 23].

The plasma acceleration mechanism in such relies on the frozen-in condition of highly-conductive plasmas[4]. This property allows the magnetic nozzle to guide the plume resembling the gas dynamic expansion in conventional rocket nozzles. The momentum is then transferred back to the thruster by the mutual interaction of induced diamagnetic currents in the plume and the applied magnetic field[17].

A central issue in MNs is plasma detachment[1, 3, 10, 15]. The same frozen-in condition tends to force the particles along the returning magnetic field lines, inhibiting plasma detachment, which is essential for

[*]Graduate Student, Politecnico di Milano; Visiting Graduate Research Assistant, Princeton University

[†]Graduate Research Assistant

[‡]Chief Scientist, EPPDyL; Professor, Applied Physics Group, Mechanical and Aerospace Engineering Department; AIAA Fellow.

creating a free thrust-producing plasma jet. Recent experiments[6, 7, 25, 22] and simulations [1, 2, 3] suggest that detachment could occur under some conditions. However, beam divergence of the plasma jet, which results in a decrease in thrust efficiency, and how to decrease it, remain an open question.

Schmit and Fisch [23] expanded Hooper's [11] magnetic nozzle model, introducing a differential azimuthal motion in the plasma populations as boundary conditions at the throat. They found that the resulting azimuthal current can couple with the axial magnetic field, producing a significant decrease in the plume divergence.

The relevance of Hooper's model to magnetic nozzle flows has been contested because it neglects electron pressure terms and assumes local ambipolarity[3]. The idea to use azimuthal currents within the source of a magnetic nozzle flow to reduce plume divergence is robust, however, as we have recently shown[9] using an approximate analytical solution[19] to the 2D MN expansion model of Ahedo and Merino[1]. By introducing a correction to the nozzle throat boundary conditions, derived by modifying the radial equilibrium of a magnetized infinite two-population cylindrical plasma column with the insertion of an external azimuthal body force for the electrons, and Including finite-temperature effects, we showed analytically that an applied azimuthal current focuses the plasma towards the nozzle axis and reduces the width of the resulting plume. Using this model we analyzed the performance improvements and suggested a focusing stage at the MN convergent section to improve thruster efficiency.

In this paper we describe an experimental proof of concept used to test the theoretical prediction of reduced plume divergence with induced azimuthal currents. A simple way of introducing an azimuthal current at the nozzle throat is to use concentric electrodes positioned right before the MN throat and coaxial with the plasma column. The interaction between the radial electric field and the axial magnetic field induces an azimuthally-directed Hall current in the plasma. The direction of this current depends on the direction of the electric field and a diamagnetic current is required for plume collimation.

The main objectives of this experimental study are: to investigate the ability of the concentric-electrodes architecture for the focusing stage to drive a steady state azimuthal current; to assess the effect of the focusing stage on the transverse density and potential distributions inside the thruster; and to verify that a net focusing effect is propagated outside in the plume.

II. Experimental Setup

II.A. Plasma Source

Our experimental investigation was performed using the magnetic nozzle experiment [14] recently built at the Electric Propulsion and Plasma Dynamics Laboratory (EPPDyL) at Princeton University, which was especially modified for the purposes of this study. The experiment shown in the photograph of Fig. 1 and the schematic of Fig. 2 consists of a helicon plasma source enclosed in a borosilicate glass tube of 37.5 mm in radius and a couple of magnetic coils for the induction of the magnetic nozzle field. The operating gas is argon, ionized and heated by means of a two-turn planar copper antenna operating at 13.56 MHz. The propellant feedline is coaxial with the antenna and goes through through a Macor backplate. The RF signal is generated by an Agilent 8648B Signal Generator. Two amplifiers (ENI 2100L pre-amplifier and Alpha 9500) in series provide up to 1 KW of RF power for ionization and plasma heating. An Alpha 4520 digital wattmeter is used to measure the standing-wave ratio (SWR) and the delivered power. No independent plasma heating stage is implemented. The antenna matching is achieved by an L-type tunable custom-built capacitor network. The plasma source is coated with a copper mesh for preventing stray RF radiation.

The nozzle electromagnets have their copper windings centered at a mean radius 75.1 mm from the axis , and are made of 144 turns (12 x 12) of AWG 10 square, copper magnet wire wrapped on an aluminum core. The coils are powered by an Amrel SPS32 DC power supply, operated in current control. The downstream electromagnet is aligned with the end of the glass tube and the magnetic nozzle throat is axially located between the two coils.

The experiment is assembled within EPPDyL's Large Dielectric Pulsed Propulsion vacuum chamber. The fiberglass chamber measures approximately 2.5 m in diameter and 7.5 m in length. The vacuum is provided by a three-stage vacuum system composed by a pait of Stokes mechanical roughing pumps, a roots blower and a CVC diffusion pump, capable of achieving pressures as low as 2×10^{-6} Torr. The antenna is water cooled, while the electromagnets are passively cooled. Thus, experimental runs are limited to two hours to avoid excessive heating of the electromagnets. Temperatures are monitored using a FLIR infrared camera.

Quantity	Value
P	$200 - 750$ W
$\dot{m}$	$0.5 - 2.0$ mg/s Ar
B	$0 - 800$ G
n	$1 - 6 \cdot 10^{18}$ m^{-3}
T_i	~ 0.5 eV
T_e	5 to 10 eV

Table 1. Typical plasma parameters of the Magnetic Nozzle experiment[18].

Typical plasma parameters associated with this experiment, operating in helicon mode, are reported in Table 1.

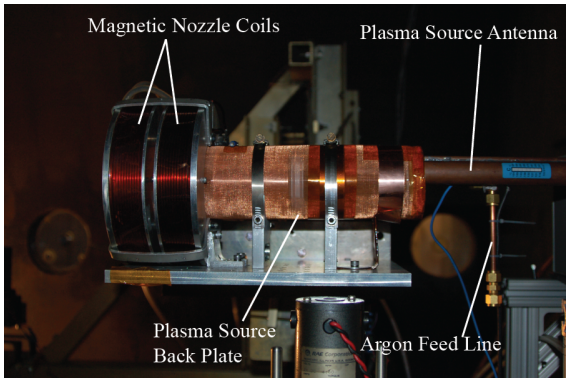

Figure 1. Photogrpah of the plasma source used for the Magnetic Nozzle experiment. Details and dimensions are shown in the schematic of Fig. 2

II.B. Diagnostics

The main diagnostic we used in this study is an RF-filtered Langmuir probe (LP) based on the design of Sudit and Chen [24]. The probe tip is made of tungsten wire with a diameter of 0.25 mm and a length of 1 mm. The RF compensation is achieved using four self-resonant chip inductors with frequencies of 14 and 28 MHz. The LP was mounted on a movable fiberglass stand with position control that allows both radial and angular degrees of freedom.

Electron temperature was calculated from the slope of the linear region in the measured current-voltage characteristic curve of the Langmuir probe. The error on the temperature measurement was estimated at 25 %[24]. Plasma density n_i was found from the ion saturation current, corrected to account for the sheath expansion[13, 20]. Plasma potential is computed from the floating potential, corrected for the electron temperature.

II.C. Focusing Stage

The focusing stage, which consists of a pair of concentric electrodes for inducing the azimuthal current, has a solid molybdenum cathode and an annular copper anode. The relevant dimensions of the experimental setup are reported in Fig. 2.

A stainless steel 6.3-mm (1/4-inch) feed line replaces the non-conducting tube of the original magnetic nozzle experiment. Two sets of four 2.25-mm azimuthal feed holes on the shaft of the central tube provide the argon feed. The the steel feeding tube is electrically grounded and the external electrode is biased positively through an electrical connection across the pyrex cylinder. The metallic feed line shields the argon from the electromagnetic waves emitted from the antenna, preventing the ionization to occur upstream of the feed holes. A longitudinal cut was made along the anode in order to avoid induced currents to flow in the azimuthal direction due to RF coupling.

III. Operation

Complete data collection required about 50 hours of discontinuous runs of the experiment. During all the operations, the argon mass flow rate was set at 2 mg/s and the backgtound pressure was 5×10^{-5} Torr (6.7 mPa) and never exceeded 1×10^{-4} Torr (13.3 mPa) during the experiments.

To characterize the effect of the electrodes on the plasma flow, two series of measurements were taken, one inside the focusing stage and one in the plume outside the thruster. For these measurements, the chosen values of magnetic field were 120, 200 and 280 G (measured with a Gaussmeter at the nozzle throat). The RF power delivered to the helicon antenna was set to 500 W for 120 G and 200 G, while an higher value of

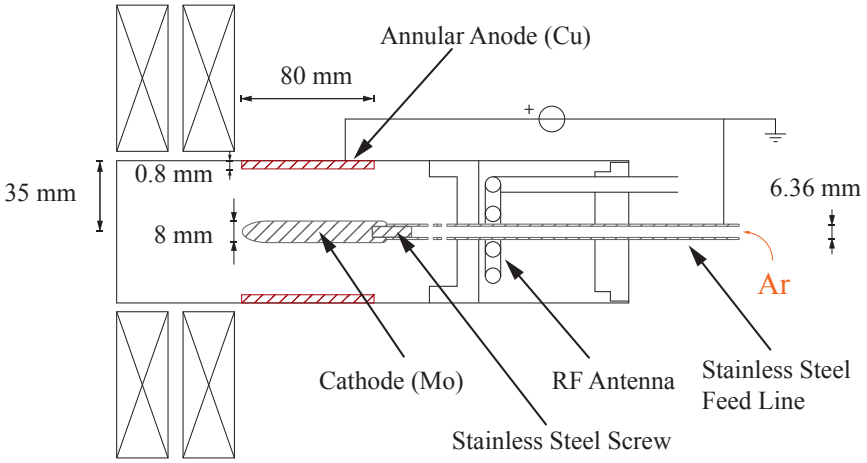

Figure 2. Schematic of the plasma source, showing materials and relevant dimensions.

600 W was chosen for operation at 280 G in order to prevent instabilities and mode transitions, which were observed at lower power.[18]

The measurements inside the plasma source were taken at four different voltages: 2 , 7 , 15 , 25 and 35 V; those in the plume were taken at 2 , 7 , 20 and 35 V. The first of these voltages (either 2 or 7 V) was set to be close to the zero-current value identified in section IV IV.A.

For the plasma characterization between the electrodes, we moved the Langmuir probe radially between the cathode and the anode. The measurements were taken every 5 mm from $r = 10$ mm (6 mm from the cathode) to $r = 30$,m (4 mm from the anode).

For measurements in the external plume, the probe was set to a distance of 20 cm from the nozzle throat and was swept through an angle of 45 degrees on one side, with measurements taken every 5 degrees. A schematic showing the measurement locations inside the focusing stage and in the external plume is shown as Fig. 3. At the 45-degree location, the arc made by the sweep is approximately perpendicular to the diverging magnetic field lines.

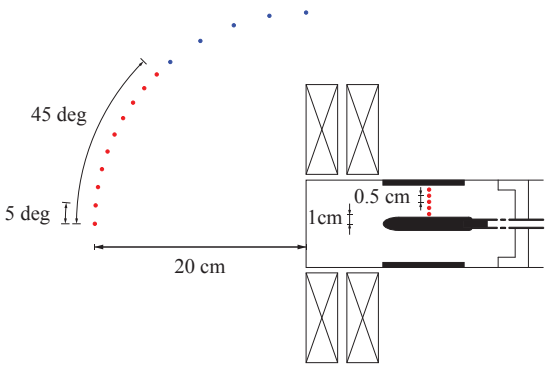

Figure 3. Locations of the Langmuir probe used for the measurements inside the focusing stage and in the external plume. Measurements in the external plume beyond 45 degrees (whose locations are shown as blue dots) showed very low density and negligible angular variation in the measured quantities, and consequently have been omitted for clarity from the results reported below.

IV. Results

IV.A. Current-Voltage Characteristic Curve

The current-voltage characteristic curve of the electrodes circuit, shown in Fig. 4, was obtained by applying the desired voltage using the DC power supply and measuring the current as a voltage drop across a calibrated resistor.

As seen in that figure, after an initially linear dependence on the voltage, the current approaches an asymptotic limit that depends on the applied magnetic field. This transition is sharper for higher magnetic fields and that there is a finite voltage for the zero-current condition, whose value depends on the applied magnetic field.

We can explain these trends as follows. At 0 G (no magnetic field) and at 0 V (shorted electrodes), both the electrodes are collecting a small electron current since their floating potential is below 0 V. Since the density is approximately constant in the radial direction and the anode area is larger than that of the

cathode, a net current flows from the anode to the cathode (positive current). When we apply a voltage, the cathode is kept a 0 V (ground) while the anode collects an increasing number of electrons until electron saturation is reached.

When we increase the magnetization, the floating potential of both electrodes becomes positive, with the anode floating potential greater than that of the cathode. At 0 V the anode collects an increasing number of ions as the magnetic field increases, eventually overcoming those collected by the cathode and leading to a net negative current. For restoring a zero-current condition, a voltage has to be applied to repel ions from the anode (i.e. moving the anode potential closer to the floating potential). The higher saturation current seen at higher magnetization is probably due to increased mobility of electrons along the magnetic field lines connecting the electrodes, increased plasma densities at larger magnetic fields, or a combination of these effects.

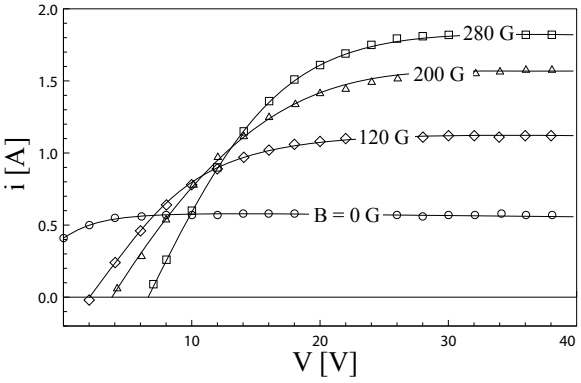

Figure 4. Current-Voltage characteristic curves of the electrodes circuit, at various magnetic field strengths. The source power is always set to 500 W, Argon mass flow rate 2 mg/s.

IV.B. Focusing of the Internal Plasma

We characterized the plasma inside the focusing stage by measuring the radial profiles of the density and potential at various applied voltages and magnetic fields. From these measurements, we can infer a relationship between the applied electric field, azimuthal current and density profile within the focusing stage.

The electron temperature was measured at 6 eV for all the operating conditions, which is consistent with previous measurements in electrodeless MN configuration of the experiment [18].

The radial density and potential profiles at various values of magnetic field and applied voltage to the electrodes are shown in Figs. 5, 6 and 7. It is clear from these plots that an increase in the voltage across the electrodes leads to a pinching of the plasma in all cases. We also see that, with lower applied voltages, the peak of the density profile moves radially outward form the center axis. Such off-axis peaks were not observed in the previous electrodeless version[18] of the plasma source, which leads us to deduce that the presence of the cathode on the center axis has a perturbing effect that lowers the plasma density in the vicinity of that axis causing an annular like distribution of plasma density. However, this perturbed distribution, as will be seen in the next section, was not observed in the external plume, suggesting that a cross-field diffusion occurs between the focusing stage edge and the nozzle throat, effectively diluting the effect of that perturbation.

The measured plasma potentials show that generally, as expected, the plasma potential increases radially away from the center axis for all applied voltages and magnetic field values, indicating that an inward-directed electric field is induced in the plasma, as desired. Also, as expected, due to electrode sheaths, the bulk plasma is always at a higher potential than the walls. Indeed, even if the cathode is grounded, the innermost plasma potential is always much higher. Thus, most of the applied voltage is actually lost near the cathode and does not penetrate the bulk plasma due to the shielding effect of the sheaths. Another potential drop is found near the anode, which we suspect is related to the anode boundary layer and pre-sheath[8].

We can infer average values of the azimuthal current density from the Hall part of Ohm's law after estimating the classical conductivity tensor $\underline{\underline{\sigma}}$ using the measured plasma parameters. Adopting the usual cylindrical coordinates and approximating the magnetic field as parallel to the z axis, the resulting conductivity tensor can be written as [16]

$$\underline{\underline{\sigma}} = \begin{bmatrix} \sigma_\perp & \sigma_H & 0 \\ -\sigma_H & \sigma_\perp & 0 \\ 0 & 0 & \sigma \end{bmatrix} \quad , \tag{1}$$

where σ is the parallel (scalar) conductivity, which we estimate using the measured plasma parameters to be $\sigma = 1.74 \cdot 10^4 \ (\Omega \cdot \mathrm{m})^{-1}$. We also calculate the other two terms of the conductivity tensor, $\sigma_\perp$ and σ_H for for each of the three magnetic field values and tabulate the results in Table 2.

As is clear from the last column of tab.2, the Hall current dominates the radial current when a radial electric field is applied to the plasma. We also note that, for a constant radial electric field, raising the

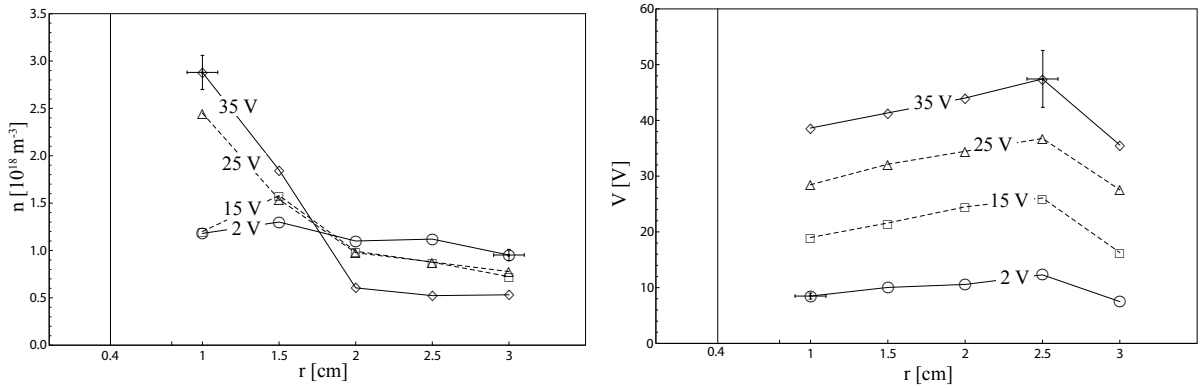

Figure 5. Radial profiles of plasma density and plasma potential between the electrodes of the focusing stage. Applied magnetic field 120 G. The vertical black line marks the border of the cathode. For clarity, only two error bars are reported.

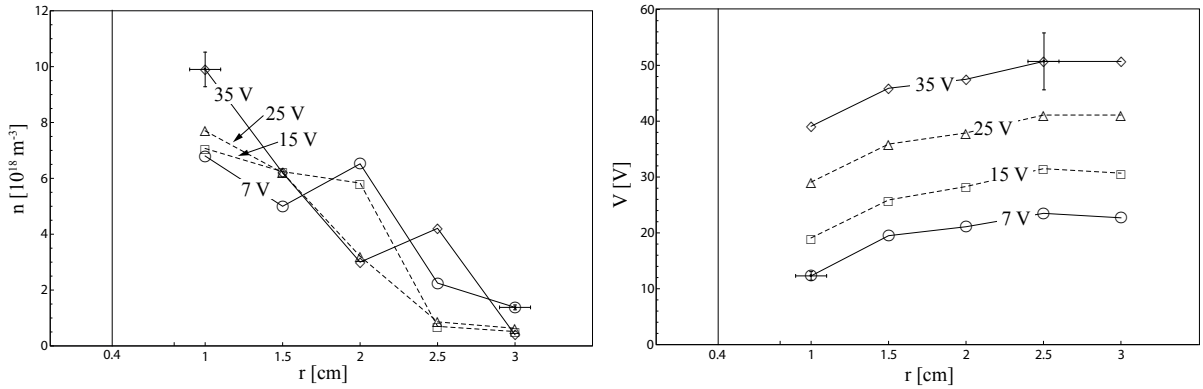

Figure 6. Radial profiles of plasma density and plasma potential between the electrodes of the focusing stage. Applied magnetic field 200 G.

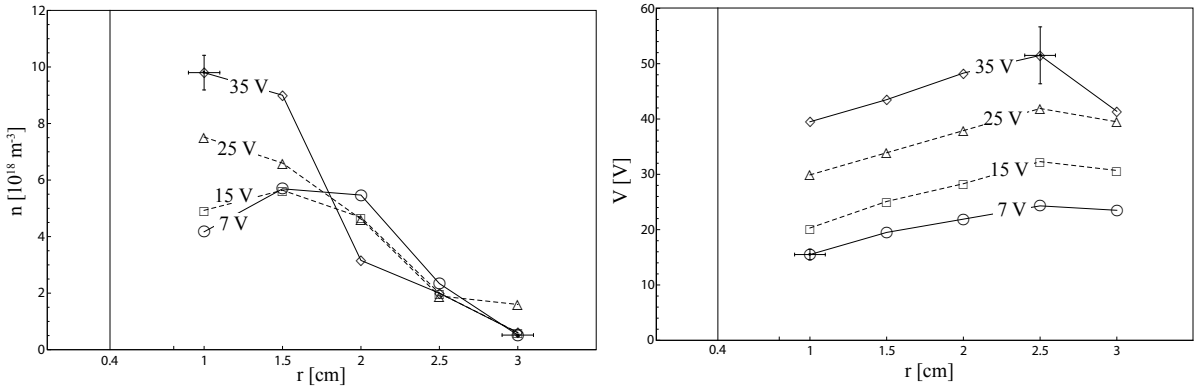

Figure 7. Radial profiles of plasma density and plasma potential between the electrodes of the focusing stage. Applied magnetic field 280 G.

B [G]	$\sigma_\perp/\sigma$	σ_H/σ	$\sigma_H/\sigma_\perp$
120	$1.907 \cdot 10^{-5}$	0.0023	120.6
200	$1.555 \cdot 10^{-5}$	0.0014	90.0
280	$1.466 \cdot 10^{-5}$	0.0010	66.85

Table 2. Perpendicular and Hall conductivities in the plasma at different magnetic fields.

magnetic field leads to a decrease in the Hall conductivity due to the increased $\mathbf{E} \times \mathbf{B}$ drift of the ions.

Using a linear fit to the plasma potential profiles we can estimate a radially-averaged value of the radial electric field, E_r, which allows us to estimate the radially averaged azimuthal current density from

$$J_\theta = -\sigma_H E_r \quad . \tag{2}$$

To depict the pinching effect of the azimuthal current we plot in Fig. 8 the ratio n_p/n_{p0} with respect to $J_\theta/J_{\theta 0}$, where n_p is the peak of the measured plasma density radial profile, n_{p0} is n_p for $J_\theta = J_\theta|_{\text{zero current}}$ and $J_{\theta 0}$ is the azimuthal current density, for the B = 120 G case, when the current in the electrode circuit is zero. It is clear from Fig. 8 that the normalized density peak value generally increases with the azimuthal current, thus demonstrating that concentric electrodes can drive an azimuthal Hall current in the plasma, and that this current leads to a focusing of the the internal plasma towards the centerline of the device.

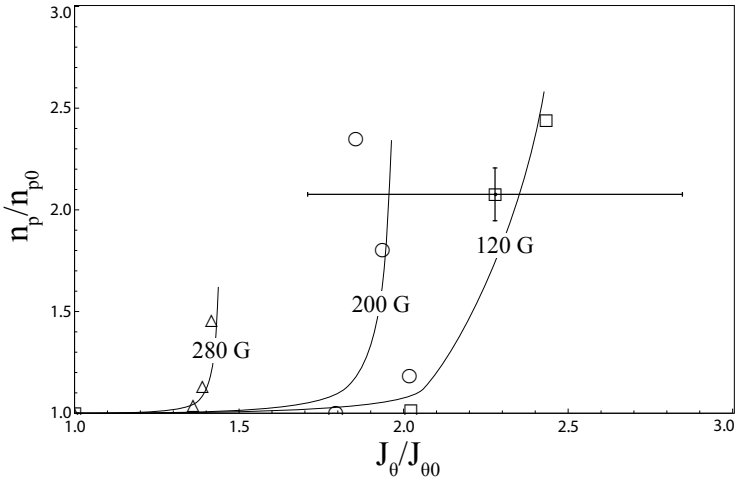

Figure 8. Normalized peak plasma density inside the plasma source as a function the induced azimuthal current density at three values of the magnetic field. Reference values n_{p0} and $J_{\theta 0}$ are at the condition where no current flows in the electrode circuit. A typical error bar is shown.

IV.C. Focusing of the External Plasma Plume

The measured angular profiles of the plasma density and plasma potential in the external plasma plume are shown in Figs. 9, 10 and 11, for different values of the magnetic field and applied voltage.

In all cases, the electric potential across the plume is approximately constant, with a minimal drop at large angles. The value of the potential increases with the applied voltage, as was the case inside the plasma source. The fact that the plasma potential increases with the applied voltage outside in the plume, far from the focusing stage, suggests that the collimation of the plasma at the nozzle throat is maintained into the plume.

From the density profile measurements we observe either an increased plasma density in the inner region (see Fig. 10), or a faster decay in the external region (see Fig. 9). The first effect is more prevalent than the second, and is a predicted result of the two-fluid expansion model modified to include the effects of induced azimuthal currents.[9].

The density profiles of the 200 G and 280 G cases demonstrate an increased density along the nozzle axis with increasing electrode bias (hence increasing azimuthal current density at fixed magnetic field), with the focusing effect being more pronounced for the 200 G case due to higher values of azimuthal current in the source (Fig. 8). Even though the 120 G case features the largest azimuthal current in the plasma source, the plume does not focus as much as the higher magnetic field cases. We believe that the diminished focusing may be due to enhanced cross-field transport at low magnetic fields [14].

Finally, we note that the power consumed by the focusing stage always remained 10 % below the RF power delivered to the plasma source. We also report that increasing the power of the plasma source by 10 % while turning off the focusing stage had very little effect on the plume. This implies that introducing additional power to the plasma flow through a focusing stage may be more effective than simply increasing the power delivered by the antenna.

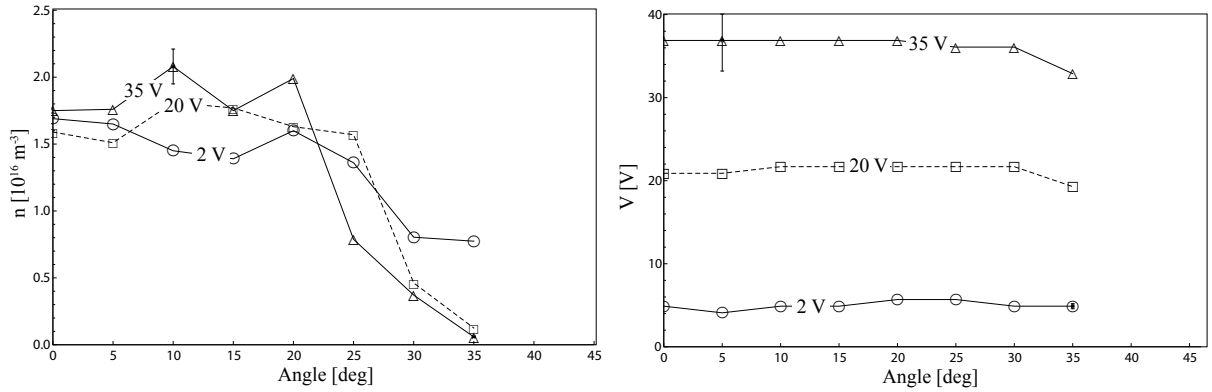

Figure 9. Angular profile of plasma density and potential in the plume at 20 cm from the nozzle throat. $B = 120$ **G. The measurements beyond 35 degrees from the axis were too noisy for a reliable density distribution estimation and have been omitted. For clarity, only two typical error bars are reported.**

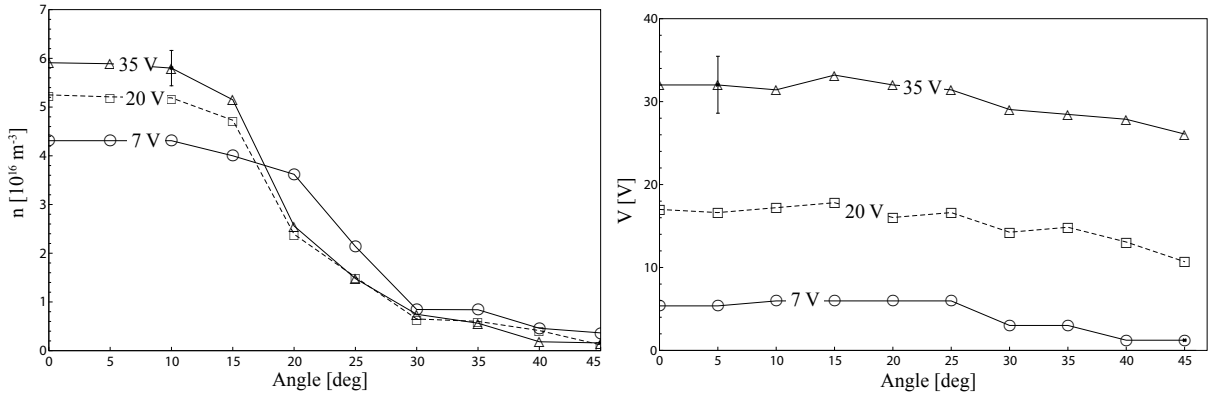

Figure 10. Angular distribution of plasma density and potential in the plume at 20 cm from the nozzle throat. $B = 200$ **G.**

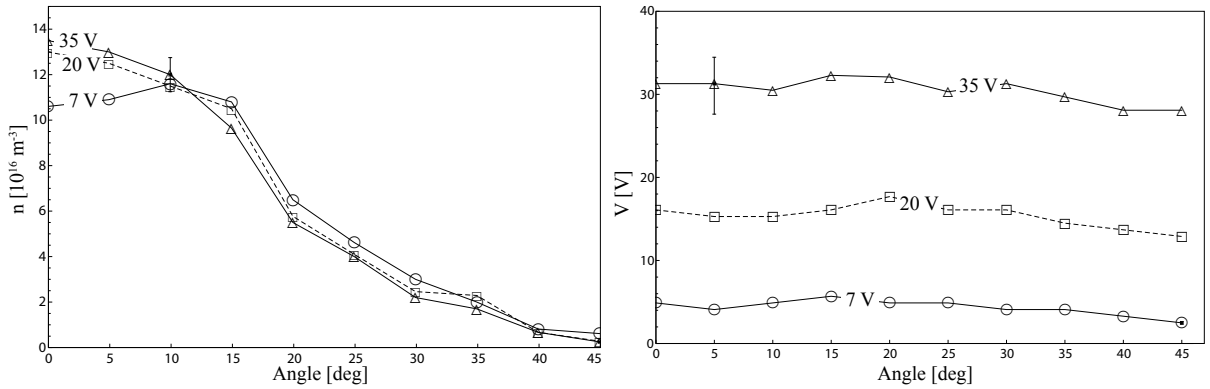

Figure 11. Angular distribution of plasma density and potential in the plume at 20 cm from the nozzle throat. $B = 280$ **G.**

V. Conclusions

The study described in this paper leads us to the following main four conclusions:

1. The theoretically predicted[23, 9] ability of an applied azimuthal current to focus the plasma in a magnetic nozzle (MN) was demonstrated experimentally by inducing such a current through the application of a radial electric field from a pair of concentric electrodes upstream of the throat and measuring the radial profiles of plasma density inside of the source and in the exhaust region.

2. As we predicted theoretically[9], the plasma focusing that occurs upstream of the throat is significantly maintained in the exhaust region far downstream of the throat.

3. The power invested in applying such a focusing azimuthal current does not lead to much plasma focusing if it were invested in the plasma generation stage.

4. A plasma focusing stage based on this scheme is a promising concept for actively controlling the beam divergence, and hence the propulsive performance, of plasma flows in magnetic nozzles.

Acknowledgments

The work of the first author has been supported by the scholarship *Borsa di Studio Tesi All'Estero 2012-2013* of the Politecnico di Milano. We also acknowledge support from Princeton's Plasma Science and Technology Program. The authors would like to thank Dr. Sam Cohen for suggesting the concentric electrode configuration for driving azimuthal current. We would also like to thank Robert Sorenson for his help in the experiment manufacturing and set up.

References

[1] E. Ahedo and M. Merino. Two-dimensional supersonic plasma acceleration in a magnetic nozzle. *Physics of Plasmas*, 17:073501, 2010.

[2] E. Ahedo and M. Merino. Magnetic nozzle far-field simulation. In *Proceedings of the 48th AIAA/ASME/SAE/ASEE Joint Propulsion Conference*, Jul 2012.

[3] E. Ahedo and M. Merino. Two-dimensional plasma expansion in a magnetic nozzle: Separation due to electron inertia. *Physics of Plasmas*, 19:083501, 2012.

[4] H. Alfvén. On frozen-in field lines and field-line reconnection. *Space Physics*, 81:4019–4021, 1976.

[5] S.A. Cohen, X. Sun, E.E. Ferraro, N.M. abd Scime, M. Miah, S. Stange, N.S. Siefert, and R.F. Boivin. On collisionless ion and electron populations in the magnetic nozzle experiment (mnx). *IEEE Trans. Plasma Sci.*, 34:792–803, 2006.

[6] W Cox, C Charles, R W Boswell, and R Hawkins. Spatial retarding field energy analyzer measurements downstream of a helicon double layer plasma. *Appl. Phys. Lett.*, 93(7):071505, 2008.

[7] Christopher A Deline, Roger D Bengtson, Boris N Breizman, Mikhail R Tushentsov, Jonathan E Jones, D Greg Chavers, Chris C Dobson, and Branwen M Schuettpelz. Plume detachment from a magnetic nozzle. *Phys. Plasmas*, 16:033502, 2009.

[8] E. Distefano and H. J. Pain. Electrical current in a moving plasma between cold electrodes. *British Journal of Applied Physics*, 2:1085–1093, 1969.

[9] L. Ferrario, J. M. Little, and E. Y. Choueiri. Propulsive performance of a finite-temperature plasma flow in a magnetic nozzle with applied azimuthal current. *Physics of Plasmas*, In Review, 2014.

[10] A. Fruchtman, K. Takahashi, C. Charles, and R.W. Boswell. A magnetic nozzle calculation of the force on a plasma. *Physics of Plasmas*, 19:033507, 2012.

[11] E. B. Hooper. Plasma detachment from a magnetic nozzle. *Journal of Propulsion and Power*, 9(5):757–763, 1993.

[12] R. Hoyt, J. Scheuer, K. Schoenberg, R. Gerwin, R. Moses, and I. Henins. Magnetic nozzle design for coaxial plasma accelerators. *IEEE Trans. Plasma Sci.*, 23:481–494, 1995.

[13] I. H. Hutchinson. *Principles of Plasma Diagnostics, Second Edition.* Cambridge University Press, Cambridge, UK.

[14] Little J.M. and E. Y. Choueiri. Critical condition for plasma confinement in the source of magnetic nozzle flows. *IEEE Transactions on Plasma Science: Special Issue on Plasma Propulsion*, Accepted, 2014.

[15] K. Kuriki and Okada O. Experimental study of a plasma flow in a magnetic nozzle. *Phys. Fluids*, 13:2262–2269, 1970.

[16] LD Landau and EM Lifshitz. Statistical physics, part i. *Course of theoretical physics*, 5, 1980.

[17] J. M. Little and E. Y. Choueiri. Plasma detachment and momentum transfer in magnetic nozzlesers. In *Proceedings of the 47th AIAA/ASME/SAE/ASEE Joint Propulsion Conference*, Jul 2011.

[18] J. M. Little and E. Y. Choueiri. Plasma transport in a converging magnetic field with applications to helicon plasma thrusters. In *Proceedings of 33rd International Electric Propulsion Conference*, October 2013.

[19] J. M. Little and E. Y. Choueiri. Thrust and efficiency model for electron-driven magnetic nozzles. *Physics of Plasmas*, 20:103501, 2013.

[20] R. L. Merlino. Understanding langmuir probe current-voltage characteristics. *American Journal of Physics*, 75:1078–1085, 2007.

[21] C.S. Olsen, M.G. Ballenger, M.D. Carter, F.R. Chang Daz, M. Giambusso, T.W. Glover, A.V. Ilin, J.P. Squire, B.W. Longmier, E.A. III Bering, and P.A. Cloutier. An experimental study of plasma detachment from a magnetic nozzle in the plume of the vasimr engine. In *Proceedings of the 33rd International Electric Propulsion Conference*, Oct 2013.

[22] C.S. Olsen, M.G. Ballenger, M.D. Carter, F.R.C. Diaz, M. Giambusso, T.W. Glover, AV. Ilin, J.P. Squire, B.W. Longmier, E.A Bering III, and P.A Cloutier. Investigation of plasma detachment from a magnetic nozzle in the plume of the vx-200 magnetoplasma thruster, 2014.

[23] P. F. Schmit and N. J. Fisch. Magnetic detachment and plume control in escaping magnetized plasma. *Journal of Plasma Physics*, 75(3):359–371, 2009.

[24] Isaac D Sudit and Francis F Chen. Rf compensated probes for high-density discharges. *Plasma Sources Sci. Technol.*, 3(2):162, 1994.

[25] K Terasaka, S Yoshimura, K Ogiwara, M Aramaki, and M Y Tanaka. Experimental studies on ion acceleration and stream line detachment in a diverging magnetic field. *Phys. Plasmas*, 17(7):072106, 2010.